Iron Pnictides and Chalcogenides: a New Paradigm for Superconductivity

Rafael M. Fernandes,[1] Amalia I. Coldea,[2] Hong Ding,[3,4]
Ian R. Fisher,[5,6] P. J. Hirschfeld,[7] and Gabriel Kotliar[8,9]

[1]School of Physics and Astronomy, University of Minnesota, Minneapolis, MN 55455

[2]Clarendon Laboratory, Department of Physics, University of Oxford, Parks Road, Oxford OX1 3PU, UK

[3]Beijing National Laboratory for Condensed Matter Physics and Institute of Physics, Chinese Academy of Sciences, Beijing 100190, China

[4]CAS Center for Excellence in Topological Quantum Computation, University of Chinese Academy of Sciences, Beijing 100190, China

[5]Geballe Laboratory for Advanced Materials and Department of Applied Physics, Stanford University, Stanford, CA 94305, USA

[6]Stanford Institute for Materials and Energy Science, SLAC National Accelerator Laboratory, 2575 Sand Hill Road, Menlo Park, California 94025, USA

[7]Department of Physics, University of Florida, 2001 Museum Rd, Gainesville, FL 32611, USA

[8]Physics and Astronomy Department, Rutgers University, Piscataway, New Jersey 08854, USA

[9]Condensed Matter Physics and Materials Science Department, Brookhaven National Laboratory, Upton, New York 11973, USA

(Dated: December 12, 2021)

Abstract

Superconductivity is a remarkably widespread phenomenon observed in most metals cooled down to very low temperatures. The ubiquity of such conventional superconductors, and the wide range of associated critical temperatures, is readily understood in terms of the celebrated Bardeen-Cooper-Schrieffer (BCS) theory. Occasionally, however, unconventional superconductors are found, such as the iron-based materials, which extend and defy this understanding in new and unexpected ways. In the case of the iron-based superconductors, this includes a new appreciation of the ways in which the presence of multiple atomic orbitals can manifest in unconventional superconductivity, giving rise to a rich landscape of gap structures that share the same dominant pairing mechanism. Besides superconductivity, these materials have also led to new insights into the unusual metallic state governed by the Hund's interaction, the control and mechanisms of electronic nematicity, the impact of magnetic fluctuations and quantum criticality, and the significance of topology in correlated states. Over the thirteen years since their discovery, they have proven to be an incredibly fruitful testing ground for the development of new experimental tools and theoretical approaches, both of which have extensively influenced the wider field of quantum materials.

A comprehensive understanding of conventional superconductors, in which lattice vibrations bind electrons in Cooper pairs, is provided by the BCS-Eliashberg theory. Several families of unconventional superconductors, however, defy explanation within this paradigm, presenting a series of rich intellectual challenges. For many years, attention was split between cuprate superconductors [1], with critical temperatures (T_c) up to 165K, and the heavy-fermion and organic superconductors, with lower T_c values [2]. In 2008, a new family of superconductors was discovered based on iron (Fe) [3]. The discovery was noteworthy given that Fe is generally seen as a strongly magnetic ion, and magnetism is typically antithetical to superconductivity. It rapidly became more remarkable as new members of the family were discovered with progressively higher T_c values – high enough that the materials were soon referred to as "high-T_c".

A large body of evidence now indicates that these Fe-based superconductors (FeSC) are unconventional, i.e. that pairing is not driven by lattice vibrations (phonons) [4–8]. They have provided a fascinating array of new insights into the conditions of occurrence and nature of unconventional superconductivity, particularly in systems where the electrons can occupy multiple orbitals. Prior to their discovery, unconventional pairing was synonymous with Cooper pairs with non-zero angular momentum and gap nodes, exemplified, for instance, by the d-wave superconducting state realized in cuprates [1]. In iron-based materials, however, the Cooper pairs are widely believed to have zero angular momentum, their unconventional nature arising from the different phases they take on different bands [4, 5]. A variety of pairing structures have been observed, but attributed to the same dominant pairing mechanism.

Besides superconductivity, the normal state of the FeSC is also unusual. Similar to many other quantum materials, electron-electron interactions play an important role in shaping their phase diagrams. However, due to the multi-orbital character of these compounds, it is the Hund's interaction that is believed to play the most prominent role [9]. The resulting "Hund metal" [10] interpolates between a description of incoherent atomic states at high temperatures and one of coherent states at low temperatures. At intermediate temperatures, charge and orbital degrees of freedom seem itinerant, while spin degrees of freedom appear localized [11]. In contrast, in the cuprates, the onsite Hubbard repulsion is the dominant interaction, whereas in heavy-fermion materials, it is the Kondo coupling between localized and itinerant electrons. Another distinguishing feature of FeSC is that although the distinct Fe orbitals are subjected to the same interactions, they experience different degrees of correlation, a phenomenon dubbed orbital differentiation [10, 12–16].

It is from this correlated normal state that not only superconductivity emerges, but also other electronic ordered states. The majority of FeSC order magnetically [17]; for example, $BaFe_2As_2$ exhibits magnetic order with a stripe pattern below a critical temperature of 134 K, although more unusual spin configurations are found under hole doping [Fig. 1(a)]. Other compounds, such as FeSe, exhibit no magnetic order at ambient pressure [Fig. 1(b)]. More ubiquitously, magnetic fluctuations at the stripe-order wave-vectors are commonly observed for superconducting compositions. The observation, by neutron scattering, of an associated resonance in the magnetic spectrum at this specific wave-vector [18, 19] has been widely interpreted as evidence for a sign-changing superconducting gap and for magnetic fluctuations playing a key role in the pairing interaction [2].

Another common feature in the FeSC phase diagrams is a tetragonal-to-orthorhombic phase transition. It often occurs either concurrently or at a higher temperature than the magnetic transition [Fig. 1(a)], although in FeSe it occurs in the absence of magnetic order at ambient pressure [Fig. 1(b)]. A variety of experiments have revealed that lattice strain is not the primary order parameter for this phase transition [20]. Borrowing language from liquid crystals, the state is referred to as an electronic nematic phase [21], in which interactions among electronic degrees of freedom drive the breaking of (discrete) rotational symmetry, while translational symmetry is unaffected. Experiments indicate that nematic fluctuations extend far across the phase diagram [22–24], motivating the question of what role nematicity plays in these materials.

The most recent surprise is the realization that several representative FeSC compounds can display topologically non-trivial band structures [25]. They have been proposed to promote various topological phenomena, such as spin-momentum-locked surface states and semi-metallic Dirac bulk states. Due to their intrinsic fully gapped unconventional superconductivity, they have become prime candidates in the search for robust topological superconducting states and their associated Majorana excitations.

The above brief overview showcases an important feature of the FeSC. After 13 years of research there is a wide consensus as to the nature of the various states found in the phase diagrams. In the Landau paradigm, these phases are characterized by the symmetries that they break, and there has been little, if any, disagreement about them. Yet, knowing what these states are is different from understanding how they arise and inter-relate with each other. This enables a series of well-posed questions that are, in some sense, much crisper than what can currently be asked for the other family of unconventional high-T_c superconductors, the cuprates [1]. In this review, we outline what is well-understood about FeSC, and pose a series of open questions that we believe are central to understanding the origins of their superconductivity.

Electronic structure and Correlations

All FeSC are characterized by a common structural motif comprising tetrahedrally coordinated Fe atoms arranged on a square lattice [Fig. 1(c)]. The coordinating ligands are typically from groups V (the pnictogens P and As) or VI (the chalcogens S, Se, Te). Parent compounds have a formal valence Fe^{2+}, corresponding to a $3d^6$ electronic configuration for an isolated atom. Bond angles vary somewhat between compounds, differing from the perfect tetrahedral angle of $109.5°$, thus leading to additional orbital splittings [Fig. 1(d)].

From a band theory perspective, the FeSC are compensated semimetals with the same number of electron-like and hole-like carriers [26]. A widely used, simplified model features a Brillouin zone corresponding to the unit cell of the square Fe lattice [shaded gray area in Fig. 1(c)]. The low lying bands form the electron and hole Fermi-surface pockets displayed in Fig. 1(e) and colored according to the orbitals that contribute the largest spectral weight [6]. More realistic models include the puckering of the As/Se atoms above and below the Fe plane, which introduces a glide plane symmetry and implies a crystallographic unit cell (and corresponding Brillouin zone) containing two Fe atoms [blue shaded areas in Figs. 1(c) and (f)] [27, 28]. Additional effects include the spin-orbit coupling [29], which splits the intersecting electron pockets in Fig. 1(f), the three-dimensional dispersion of the bands, [27], and the hybridization between the As/Se p and Fe d bands [30], which is the root of several topological phenomena.

In the FeSC the charge and orbital degrees of freedom appear to be itinerant, as most compounds are metallic at all temperatures. Moreover, the x-ray absorption spectrum of the unoccupied Fe d states is in good agreement with DFT (density functional theory) calculations [31]. At low temperatures, the normal state of the FeSC is well described by the Fermi liquid theory. This does not imply the absence of electronic correlations, which can strongly renormalize the Fermi liquid parameters, making them deviate from DFT-based expectations. Indeed, the qualitative features of the quasiparticles dispersion, predicted by DFT and sketched in Fig. 1(e), are often similar to those detected experimentally using ARPES (angle-resolved photo-emission spectroscopy) [32–34] and quantum oscillation measurements [33, 35, 36]. However, the bandwidth of the quasiparticles dispersions are generally reduced relative to the DFT results. Such mass enhancements, also observed in optical conductivity measurements [37], are attributed to electronic correlations, and were anticipated by DFT+DMFT (dynamical mean-field theory) calculations [38–42]. Moreover, the sizes of the Fermi pockets are smaller in experiments [36, 43, 44] as compared to the DFT predictions. Whether the correlations causing this effect are promoted by low-energy spin fluctuations [44–46] or can be captured by first-principles calculations going beyond DFT [47] remains under debate.

The correlations arise from the screened Coulomb repulsion between electrons, resulting in an on-site Hubbard repulsion U, which penalizes the system when two electrons occupy the same site and suppresses spin fluctuations. However, because multiple orbitals are available in the FeSC, other on-site terms are also generated by the Coulomb repulsion. Among them is the Hund's interaction J_H, which favors the alignment of the spins of electrons in different orbitals. In contrast to the Hubbard U, J_H is barely screened from its atomic value [48]. The resulting Hund metal state differs from a Mott insulator, in that charge/orbital degrees of freedom are itinerant, while spins remain nearly localized down to low temperatures. This is illustrated schematically in Fig. 2(c), which depicts the histogram of all possible $3d$-Fe atomic states in a Hund metal. While the histogram extends over a wide range of electronic occupations, showcasing the itinerant nature of the charge carriers, it also displays sharp peaks at high-spin configurations, illustrating the local nature of the spins.

A prime feature of the Hund metal phase is the coherence-incoherence crossover [9]. In very clean FeSC, this manifests in the resistivity behavior, which crosses over from the characteristic Fermi-liquid T^2 dependence at low temperatures to values of the order of several $100\ \mu\Omega \cdot \mathrm{cm}$ at high temperatures [49]. In a semiclassical treatment, these values imply a mean-free-path comparable to the inverse Fermi momentum, inconsistent with a picture of propagating Bloch waves.

Another manifestation of the coherence-incoherence crossover is illustrated in Fig. 2(a)-(b). At high temperatures, the d_{xy} hole-band is much fainter and flatter than the two d_{xz}/d_{yz} hole-bands, reflecting the small coherence factor and large effective mass of the former. Upon decreasing the temperature, this d_{xy}-band becomes much sharper and thus more coherent. Such an effect, predicted theoretically [14, 15, 50], was observed in $FeSe_{1-x}Te_x$, LiFeAs, and $K_xFe_{2-y}Se_2$, among others [34]. In extreme cases, the d_{xy} orbital could remain completely localized down to zero temperature, while the d_{xz}/d_{yz} orbitals remain coherent, giving rise to an orbital-selective Mott state [12, 14] that behaves differently from a renormalized Fermi liquid. The fact that the d_{xy} orbital is less coherent than the others is an example of a broader phenomenon called orbital differentiation [10, 13, 51], by which different orbitals are affected by correlations in distinct ways in both the normal [15] and superconducting states [52, 53]. Orbital differentiation has been invoked to explain the strong anisotropy of the superconducting gap observed in FeSe [54]. However, the origin of this anisotropy and its relationship to orbital order remain unsettled [51, 53, 55, 56].

Correlations also affect the spin-excitation spectrum probed by neutron scattering, which is rather different at low and high energies [17]. In momentum space, as sketched in Fig. 2(d), the magnetic spectral weight at low energies is strongly peaked near the wave-vector of the magnetic ground state – usually, the in-plane stripe vectors $(\pi, 0)$ and $(0, \pi)$. As the energy increases, the magnetic spectral weight generally moves towards (π, π) [57].

This dichotomy between low and high energies is clearly seen in the local magnetic susceptibility extracted from neutron scattering experiments [17], whose imaginary part is schematically plotted in Fig. 3(a). At energies E_0 of about 100 meV, it displays a broad peak indicative of a large local fluctuating magnetic moment. Evidence for local moments are also observed in the x-ray emission spectrum, whose changes with temperature and doping have also been interpreted in terms of a spin-freezing crossover [58]. Experimental estimates give a fluctuating moment of about 2-3μ_B across different parent compounds [inset of Fig. 3(a)]. In contrast, at energy scales of about 10 meV, the imaginary part of the local susceptibility in the paramagnetic state increases with energy [59], indicative of Landau damping caused by the decay of spin fluctuations into particle-hole excitations – a hallmark of itinerant magnets. Indeed, the system remains metallic inside the magnetically ordered state.

Thus, while charge/orbital degrees of freedom are itinerant, the spin degrees of freedom display properties typical of local-spin systems at high energies and of itinerant-spin systems at low energies. This "orbital-spin" separation [11] is the most striking feature of the Hund metal. As the temperature is lowered, this correlated metallic state displays Fermi liquid behavior and an ordered phase emerges – magnetic, nematic, or superconducting. Understanding them requires considering both the Fermi surface details [Fig. 1(e)] and the magnetic spectrum [Fig. 3(a)].

Magnetism at the crossroads of itinerancy and localization

The vast majority of FeSC parent compounds, as $BaFe_2As_2$ in Fig. 1(a), undergo a magnetic transition to a stripe-like configuration [17], which consists of parallel spins along one in-plane Fe-Fe direction and antiparallel along the other [Fig. 3(b)] . There are two energetically equivalent stripe states, related by an in-plane $90°$ rotation in real and spin spaces. The spin-orbit coupling generates magnetic anisotropies that force the spins to point parallel to the selected ordering vector

[60], opening a a spin gap in the local magnetic susceptibility at low energies [Fig. 3(a)].In contrast to the fluctuating moment, the ordered moment can be rather small, and changes considerably across different compounds [inset of Fig. 3(a)] [18]. Parent compounds such as LiFeAs and FeSe, which do not undergo a magnetic transition, still display low-energy fluctuations associated with the stripe state [61, 62]. Even in FeTe, which displays a different magnetic configuration – the double-stripe state of Fig. 3(c), magnetic fluctuations at the single-stripe wave-vectors emerge upon modest substitution of Se for Te [63, 64].

Perturbations such as doping, isovalent chemical substitutions, and pressure tend to reduce the magnetic transition temperature of the pristine compositions [Fig. 1(a)] and can also give rise to new magnetic ground states. Locally, impurities can promote puddles of Néel and other orders [65]. Globally, doping $BaFe_2As_2$ with electrons stabilizes an incommensurate stripe order [66], whereas hole-doping promotes the so-called C_4 magnetic phases [67]. The latter are combinations of the magnetic configurations with different stripe wave-vectors that preserve the tetragonal (i.e. C_4) symmetry of the lattice [68, 69]. They can be either the non-collinear spin-vortex crystal [Fig. 3(d)], as observed in electron-doped $CaKFe_4As_4$ [70], or the non-uniform charge-spin density-wave [Fig. 3(e)], as observed in hole-doped $SrFe_2As_2$ [67] (see Fig. 1(a)).

The simultaneous presence of features commonly associated with localized and itinerant magnetism has motivated theoretical models adopting both a strong-coupling perspective [71–73], usually based on significant exchange interactions beyond nearest-neighbor spins, and a weak-coupling approach [13, 74, 75], often associated with Fermi-surface nesting. Nesting refers to the situation when the hole and electron pockets in Fig. 1(e) have comparable shapes and sizes. Deterioration of the nesting conditions was invoked to explain and anticipate the onset of C_4 magnetic phases and of incommensurability with doping [75]. DFT has also been widely employed to investigate magnetism in FeSC. While DFT successfully captures the magnetic ground state configuration of most compounds [4, 76], it has problems in explaining the size of the ordered moment or the absence of magnetism in FeSe [77]. Advanced, beyond-DFT *ab initio* methods, have been able to address some of these problems [10, 78].

Magnetism in FeSC also provides a new arena to explore quantum criticality [79]. A quantum critical point (QCP) is a zero-temperature second-order phase transition tuned by pressure, composition, or strain. The fact that the stripe magnetic transition temperature extrapolates to zero near the point where the superconducting dome is peaked [Fig. 1(a)] is reminiscent of certain heavy-fermion materials [2]. Quantum criticality in those compounds is empirically associated with non-Fermi-liquid behavior, such as a resistivity whose temperature dependence deviates from the standard metallic T^2 behavior at low temperatures. Note, however, that this behavior can also arise due to other mechanisms besides a QCP. Among the FeSC, $BaFe_2(As_{1-x}P_x)_2$ [Fig. 1(a)] displays the clearest evidence for strange metal behavior associated with a putative QCP. There, a linear-in-T resistivity accompanied by a mass enhancement and an unusual scaling of the magneto-resistance are observed above T_c near optimal doping [80, 81]. Below T_c, a sharp peak of the $T = 0$ superconducting penetration depth is observed near the extrapolated QCP [80], whose origin remains unsettled [82, 83].

Electronic nematicity and vestigial orders

While on symmetry grounds the nematic transition seen in most FeSC is no different than a tetragonal-to-orthorhombic transition, the driving force can arise from various mechanisms. Generally, one can define order parameters that break the tetragonal symmetry of the system in different channels – spin, orbital, and lattice [Figs. 4(a)-(c)] [20]. Symmetry requires that all of these are simultaneously non-zero or zero, but cannot determine which is the primary one. Indeed, direct experimental manifestations of nematic order have been reported in orbital [34], magnetic [84], and elastic [23] degrees of freedom, with associated anisotropies in transport [85], optical [86] and local electronic properties [87]. A crucial insight came from the realization that strain is either the primary order parameter – in which case the nematic transition would be a simple structural instability – or a conjugate field to it – in which case the instability would be electronically driven. Elasto-resistivity [22], Raman [24] and elastic stiffness measurements [23] settled this issue, establishing the dominant low-energy electronic character of the nematic state. Nevertheless, coupling to the lattice raises the critical temperature by a small amount from T^0_{nem} to T_{nem} [Fig. 4(d)].

Two general electronic mechanisms for the nematic transition have been proposed, attributing it primarily to either spin or orbital degrees of freedom. This distinction, however, can become subtle, since they can work in tandem [44, 88]. In the simplest realization of the orbital scenario, interactions spontaneously lift the degeneracy between the d_{xz} and d_{yz} orbitals [89, 90], distorting the Fermi surfaces in Fig. 1(e). In contrast, the spin scenario relies on the proximity to the stripe magnetic instability, which breaks both the (discrete) rotational and translational symmetries of the lattice [20, 91, 92]. The idea is that the stripe magnetic phase melts in two stages, first restoring the broken translational symmetry and then the four-fold rotational symmetry. The intermediate paramagnetic-orthorhombic phase that onsets between the magnetic-orthorhombic and paramagnetic-tetragonal phases is the electronic nematic. Being a partially-melted magnetic phase, this has been dubbed a "vestigial" phase of the stripe magnetic state [93]. Theoretically, because it is stabilized by magnetic fluctuations, vestigial nematicity can be captured by phenomenological, beyond mean-field Ginzburg-Landau analyses. Microscopically, it has been found in both localized spin [91, 92, 94] and itinerant magnetic [44, 95] models.

The spin-driven mechanism naturally accounts for the close proximity between the stripe-magnetic and nematic phase boundaries observed in most FeSC. Whether these two transitions are split or simultaneous, second-order or first-order, depends on doping and pressure [96]. Direct experimental evidence for this scenario is the scaling between the shear modulus C_s and the NMR spin-lattice relaxation rate $1/T_1$, suggestive that the lattice softening is caused by magnetic fluctuations [97]. Application of this mechanism to FeSe is problematic [98], however, since stripe-magnetic order is absent at ambient pressure [99] or upon S substitution [Fig. 1(b)]. The orbital-order scenario also faces challenges, at least in its simplest form, since ARPES measurements indicate the inadequacy of simple on-site ferro-orbital order [100].

The existence of a doping-dependent nematic transition also opens the possibility of a nematic QCP. Several theoretical studies point to possible exotic non-Fermi-liquid behavior near such a QCP, with implications for the description of the normal state from which the superconductor emerges [101, 102]. Probing this, however, is challenging because of its proximity to a putative magnetic QCP in most FeSC. The very nature of the coupled nematic-magnetic quantum phase transitions remains unsettled both experimentally and theoretically. Nevertheless, recent data unveiling power-law scaling of the nematic critical temperature as it is suppressed by doping and strain provides strong evidence for a nematic QCP in $BaFe_2As_2$, with an associated quantum critical regime that spans a large part of the phase diagram [103]. Another promising arena to study nematic quantum criticality is $FeSe_{1-x}S_x$ [51, 104] [Fig. 1(b)], where magnetic order is absent. Experimental evidence for possible non-Fermi-liquid behavior near the nematic QCP remains controversial, however [104, 105].

Unconventional superconducting states

The FeSC display a wide range of superconducting transition temperatures, as illustrated in Fig. 5(a). The largest $T_c \approx 65$ K is observed in monolayer FeSe grown on $SrTiO_3$, but the precise temperature where phase-coherent superconductivity sets in remains under dispute [106]. Several unsubstituted compounds display superconductivity, such as bulk FeSe, LiFeAs, and $CaKFe_4As_4$. In others, such as $BaFe_2As_2$ and LaFeAsO, the competing magnetic and nematic orders need to be suppressed, e.g. via doping, chemical substitution, or pressure, to obtain superconductivity [Figs. 1(a) and (b)]. In some compounds, a second superconducting dome can be accessed by pressure or doping [107]. In all cases, NMR measurements support a singlet pairing state.

Because the DFT-calculated electron-phonon coupling cannot account for the T_c of the FeSC [38, 108], an electronic mechanism has been proposed [6–8]. However, this does not preclude phonons, which can be enhanced by correlations [109], from playing a role in superconductivity, as it has been proposed in monolayer FeSe [110]. Quite generally, electronic repulsion forces the gap function to change sign in real/momentum space. For a large Fermi surface, like the cuprates, this can be accomplished by an anisotropic gap (e.g. d-wave). For multiple small Fermi pockets, like the FeSC, the gap can remain nearly isotropic around each Fermi surface, as long as it acquires different signs (i.e. phases) on different pockets. We refer to any gap structure that satisfies this criterion as s^{+-}-wave. In the FeSC, a strong repulsive pairing interaction is believed to be promoted by magnetic correlations associated with the nearby stripe magnetic state [Fig. 1(a)] [4]. In a weak-coupling approach, which can be implemented via RPA (random phase approximation) or (f)RG [(functional) renormalization group] calculations, the inter-pocket interaction is boosted by spin fluctuations peaked at the stripe wave-vectors $(\pi, 0)$ and $(0, \pi)$, which connect the hole and electron pockets, thus overcoming the intra-pocket repulsion [6, 7, 111]. In a strong-coupling approach, real-space pairing is promoted by the dominant next-nearest-neighbor antiferromagnetic exchange interaction [32, 71, 72]. Despite their differences, both approaches generally give an s^{+-} gap with opposite signs on the electron and hole pockets.

Besides stripe magnetism, nematic order is also strongly suppressed in the region of the phase diagram where T_c is the largest [Figs. 1(a)-(b)]. This has led to an important question that remains unresolved: what role do nematic fluctuations play for the pairing state of the FeSC [20]? Theoretically, nematic fluctuations generate an attractive pairing interaction peaked at zero momentum. Hence, they can boost T_c of any pairing state promoted by a more dominant pairing interaction (e.g. due to spin fluctuations). Nematic fluctuations can plausibly promote superconducting order on their own, particularly near a QCP [101, 102]. However, in the clearest case of $FeSe_{1-x}S_x$ [Fig. 1(b)], no strong change in T_c is observed at the putative nematic QCP [104], an issue that remains under investigation [105, 112].

Traditional phase-sensitive experiments face difficulties in distinguishing the s^{+-} from the more conventional s^{++} state, which has also been proposed as mediated by orbital fluctuations [113], because the Cooper pairs have zero angular momentum in both cases. Nevertheless, phase-sensitive setups using composite loops of polycrystalline FeSC [114] or STM quasiparticle interference [51, 115] strongly support the s^{+-}-wave state. The strongest evidence for an s^{+-} gap is the observation of a resonance mode in the magnetic susceptibility below T_c [18, 19], manifested as a sharp peak at the stripe wave-vectors and at an energy $E_{\mathrm{resonance}}$ below twice the gap value, 2Δ [schematically illustrated in Fig. 3(a)]. Such a feature is naturally explained if the gaps at momenta separated by the stripe wave-vectors have opposite signs [2]. Additional indirect evidence comes from experiments that introduce controlled disorder via irradiation. Specifically, the lifting of accidental nodes by disorder and the observed rate of suppression of T_c with impurity scattering are consistent with an s^{+-} state [116]. Moreover, the observation of in-gap bound states at non-magnetic impurities is also a hallmark of a sign-changing gap [117].

Various gap structures can be realized under the s^{+-}-wave umbrella, depending on details of the Fermi surface and on the orbital degrees of freedom [6, 7, 111]. While the gap generally has opposite signs on electron and hole pockets, additional sign changes between same-character pockets may occur [57]. Moreover, while ARPES observes nearly isotropic gaps in many compounds [32], accidental nodes may occur as well [118], which are well described by weak-coupling models [5, 6]. Some of these gap structures are illustrated in Fig. 5(b) in the 1-Fe Brillouin zone. They represent the leading gap-structure candidates of the materials in Fig. 5(a), partly motivated by theoretical considerations, but consistent with ARPES, STM, and/or neutron scattering measurements. The variety of gap structures in Fig. 5(b) and the wide range of T_{c} values in Fig. 5(a) raise the question of whether there is really a common, dominant pairing mechanism in the FeSC. Evidence in favor of this comes from the dimensionless ratio $2\Delta_{\max}/\left(k_B T_{\mathrm{c}}\right)$, where $\Delta_{\max}$ is the zero-temperature value of the largest gap. As shown schematically in Fig. 5(c), this ratio falls between 6.0 and 8.5 for many FeSC (blue shaded region) [119], in contrast with the 3.5-4.5 range observed in canonical electron-phonon superconductors (red shaded region).

The multi-band nature of the FeSC also opens the door for more exotic pairing states besides s^{+-}. This is illustrated by a toy model with one hole and two electron pockets subjected to repulsive pairing interactions. Fig. 5(d) shows schematically the pairing states obtained upon tuning the ratio between the inter-band electron-pocket/electron-pocket and electron-pocket/hole-pocket interactions, which can be different e.g. if the orbital compositions of the pockets are distinct. When the ratio is small, an s^{+-} state is obtained: the gaps on the electron pockets are identical and have a π phase shift with respect to the hole-pocket gap. When the ratio is large, a d-wave state emerges: the gaps on the two electron pockets have equal magnitude but a relative π phase, whereas the anisotropic gap on the hole pocket averages to zero. When the ratio is of order one, it is possible to realize a nematic $s + d$ superconducting state [75], in which the electron-pockets gaps have the same phase but distinct magnitudes. This is different from the case where nematicity onsets separately above T_c, as in FeSe. Another option is a time-reversal symmetry-breaking (TRSB) $s + id$ state [120], in which the electron-pockets gaps have equal magnitude but their relative phase is neither 0 (as in an s^{+-} state) nor π (as in a d-wave). A different type of TRSB pairing state, called $s + is$ [121], has been proposed in heavily K-doped $BaFe_2As_2$, based on muon-spin rotation measurements [122].

More broadly, the variation of orbital spectral weight along the Fermi pockets [Fig. 1(e)] endows the projected pairing interaction with an angular dependence, which can favor non-s-wave pairing. Microscopic calculations have in fact suggested that the s^{+-} and d-wave interactions can be comparable in strength [6, 7, 111]. Experimentally, peculiar peaks observed in the Raman spectrum have been interpreted as collective d-wave excitations inside the s^{+-} state [123, 124]. Alternatively, they have also been attributed to a collective nematic excitation [125]. The non-monotonic evolution of T_c with pressure in KFe_2As_2 has also been interpreted as evidence for nearly-degenerate superconducting states [126]. Finally, the fact that the small Fermi energy of some FeSC is comparable to the gap value has motivated the search for strong-coupling superconductivity described by the Bose-Einstein condensate (BEC) prescription of tightly-bound pre-formed Cooper pairs. Although certain properties of FeSe and $FeTe_{1-x}Se_x$ have been described in terms of a BEC-BCS crossover [104, 127], direct evidence for pre-formed pairs remains to be seen.

Topological phenomena

One of the most recent developments in the field is the discovery of topological properties in some FeSC. As schematically illustrated in Fig. 6(a), this arises from p-d band inversions along the Γ-Z direction involving an odd-parity anionic p_z-band and an even-parity Fe d-band (t_{2g}) [25]. Bulk band inversion was observed by ARPES [30, 128], but in a renormalized electronic dispersion as compared to DFT predictions [30]. The crossings of the p_z-band with the d_{xy}-band and the spin-orbit-coupling mixed $d_{xz,\uparrow} + id_{yz,\uparrow}$ band are protected, resulting in bulk topological Dirac semimetal states (blue shaded region). However, the crossing with the $d_{xz,\uparrow} - id_{yz,\uparrow}$ band is gapped, resulting in a topological insulating state (orange shaded region). Both the bulk Dirac semimetal states and the helical surface Dirac cones emerging when the chemical potential crosses the topological gap were observed by ARPES in a few FeSC, most notably $FeTe_{1-x}Se_x$ [25, 129].

Upon emergence of the s^{+-}-wave state in the bulk, superconductivity can be induced on these Dirac surface states [right panel of Fig. 6(a)]. Similarly to topological insulator/superconductor heterostructures, the surface Dirac states of the FeSC can also support Majorana zero modes (MZM) in the vortex cores of the superconducting state. Importantly, the topological superconductivity on the FeSC surface is intrinsic, displays high T_c values, and avoids the interfacial complexities of the heterostructures.

Inside the vortex of any superconductor, there are discrete energy levels of $\nu\Delta^2/E_\mathrm{F}$, where E_F is the Fermi energy. They can only be resolved in the quantum limit, where thermal broadening is smaller than the level spacing. As discussed above, FeSC usually have small E_F due to correlations. In $FeTe_{1-x}Se_x$, E_F can become comparable to Δ, making the quantum limit achievable. In an ordinary vortex, ν is expected to be half-integer, and the discrete levels never have zero energy [upper panels of Fig. 6(b)]. However, in a topological vortex, ν is shifted to integer values due to the spin texture of the Dirac states [130]. As a result, a MZM emerges as the vortex bound state with zero energy [lower panels of Fig. 6(b)]. Experimentally, both zero-energy bound states and higher-energy discrete levels have been observed in $FeTe_{1-x}Se_x$ via STM measurements [130–132], providing strong support for the existence of MZM.

Notwithstanding its simplicity, the FeSC Majorana platform is subjected to issues such as spatial inhomogeneity and the inter-layer coupling in bulk crystals. Some of these issues may be the reason why zero modes are only observed in a fraction of the vortices [130]. Besides in the interior of vortices, signatures consistent with Majorana fermions have also been observed in different types of lattice defects, such as interstitials [133], line vacancies [134], and crystalline domain boundaries [135], where a one-dimensional dispersing Majorana mode was reported. On the theory front, several ideas have been put forward for realizing other exotic topological effects, such as dispersing Majorana fermions [136] and higher-order Majorana modes in corners and hinges of samples [137].

Outlook

After 13 years, FeSC continue to provide a rich and unmatched framework to assess the interplay between correlations, unconventional superconductivity, magnetism, nematicity, quantum criticality, and topology. While significant advances have occurred, deep questions linger and continue to emerge. The correlation effects in FeSC, which are primarily driven by the Hund's interaction, appear to be enhanced upon hole doping [49]. Although several factors affect the strength of correlations [10], this observation has also been interpreted in terms of a proximate Mott insulator [71] that would exist for d^5 compositions [15, 138], analogous to the Mott state of half-filled parent cuprates. Effects typically associated with Mott physics, such as Hubbard bands, have been proposed even in d^6 compounds [139]. However, experimental observation of such a Mott state has remained elusive, leaving the interplay between Mott insulating and Hund metallic states an open question.

Understanding how and why the different ordered states – superconducting, nematic, and magnetic – emerge remains a challenge. While different approaches are possible, in the Hund-metal description this generally happens in the regime where charge degrees of freedom are itinerant but spins are localized. Explaining the phase-transitions mechanisms in this regime will require the development of novel ideas that can seamlessly combine long-wavelength, low-energy physics with local, intermediate-energy physics. The former is captured by perturbative methods such as (f)RG and RPA, which focus on the momentum dependence of the interactions and on the resulting instabilities as the system. The latter is well described by DMFT approaches that focus on the frequency dependence of the interactions.

The discovery of the FeSC provided a new arena where to test and develop *ab initio* methods for correlated electron materials [10, 40, 41, 78, 138, 140]. They proved to be of immense value for suggesting new concepts and aiding the interpretation of experiments. This line of research will continue to play an ever important role in the future, potentially assisting in the discovery of new compounds with desirable properties.

Another problem that will benefit from these first-principles correlated approaches is the elucidation of the topological properties of FeSC, as most of the existing analyses rely on DFT. More broadly, it will be invaluable to better understand how correlations and other electronic states, such as nematicity and magnetism, impact and are impacted by topological states [141]. Experimental progress will benefit from controllable tuning of MZM in the vortex state of homogeneous compounds and from designing a feasible pathway for braiding them [142].

As for antiferromagnetism and nematicity, while their symmetry-breaking properties are well understood, key issues remain unresolved, such as the origin of nematicity in Fe-chalcogenides or the role of the C_4 magnetism in Fe-pnictides. Moreover, it is still unclear whether quantum criticality is a central ingredient to the FeSC. Experimentally disentangling signatures from putative nematic and magnetic QCPs will be an important step towards elucidating this issue. Theoretically, a full description of the nematic QCP, and of its impact on the superconducting instability, will require incorporating two often neglected lattice effects. The first comes from lattice vibrations, which mediate long-range nematic interactions capable of suppressing critical fluctuations [112, 143]. The second arises from random local strains caused by dopants and other defects ubiquitously present in the samples [144, 145]. Promoting effects typical of the random-field Ising model, random strains have been argued to cause a deviation from Curie-Weiss behavior of the nematic susceptibility [146]. The related issue of electronic inhomogeneity and phase-separation is not covered in this review.

Important questions about superconductivity also remain open, despite significant theoretical progress, particularly in multi-orbital weak-coupling approaches. They include establishing how the gap structure and T_c depend on materials parameters, such as the $FeAs_4$ tetrahedral angle or the correlation-driven mass enhancement, and explaining the seemingly universal $2\Delta_{\mathrm{max}}/\left(k_B T_{\mathrm{c}}\right)$ ratio. Another challenge is posed by compounds with only hole pockets (such as KFe_2As_2) or only electron pockets (such as monolayer FeSe), which do not fall within the standard weak-coupling s^{+-} paradigm, and for which the relevance of magnetic fluctuations is not well established. Yet, both display superconductivity, with some of the electron-pocket-only compounds displaying the highest T_{c}'s among all FeSC. This begs for new approaches that can elucidate the pairing mechanism in these compounds (see e.g. [147]) and its relationship with other FeSC.

New opportunities to address some of these unanswered questions and venture into unexplored directions are provided by new iron-based compounds, which continue to be regularly discovered. Some of them have unusual structural properties due to their spacing layers, such as $CaKFe_4As_4$ with centers of inversion away from the FeAs layer, the monoclinic $Ca_{1-x}La_xFeAs_2$ [148] with a metallic spacer layer, and the insulating ladder compound $BaFe_2Se_3$ [149, 150]. Conversely, many of the theoretical and experimental advances spurred by FeSC studies have found fertile ground in other quantum materials. For instance, Hund metal concepts have been used to explain the normal-state properties of various quantum materials, most notably Sr_2RuO_4 [16]. Multi-orbital pairing models have been extensively employed to elucidate multi-band superconductors such as ruthenates and nickelates. The concept of vestigial orders and the associated phenomenological models have led to important new insights into antiferromagnetic and topological superconducting materials [93]. Experimentally, symmetry-breaking strain has been recognized as a uniquely appropriate tool to probe electronic nematic order. Strain-based techniques applied to transport, thermodynamic, scattering, spectroscopic and local probe measurements are now considered mainstream. They have enabled the identification and manipulation of electronic nematicity and a variety of other electronic states in disparate materials such as cuprates and f-electron systems. Overall, the constantly evolving toolbox developed and refined in FeSC studies has equipped the community with powerful methods to both revisit old problems and scout for new quantum electronic phenomena.

We thank all our co-authors and collaborators with whom we had many fruitful discussions since the discovery of the iron-based superconductors. We particularly thank H. Miao and T. H. Lee (Figure 2), M. Christensen (Figure 4) and L.-Y. Kong (Figure 6) for their assistance in making some of the figures. R.M.F. was supported by the U.S. Department of Energy, Office of Science, Basic Energy Sciences, Materials Science and Engineering Division, under Award No. DE-SC0020045. A.I.C. acknowledges an EPSRC Career Acceleration Fellowship (EP/I004475/1) and the Oxford Centre for Applied Superconductivity (CFAS) for financial support. A.I.C is grateful to the KITP program *correlated20*, which was supported in part by the National Science Foundation under Grant No. NSF PHY-1748958. H.D. is supported by the National Natural Science Foundation of China (Grant Nos. 11888101, 11674371), the Strategic Priority Research Program of Chinese Academy of Sciences, China (Grant Nos. XDB28000000, XDB07000000), and the Beijing Municipal Science & Technology Commission, China (Grant No. Z191100007219012). I.R.F. was supported by the Department of Energy, Office of Basic Energy Sciences, under contract DE-AC02-76SF00515. P.J.H. was supported by the U.S. Department of Energy, Office of Basic Sciences under Grant No. DE-FG02-05ER46236. G.K. was supported by NSF DMR-1733071.

---

[1] B. Keimer, S. A. Kivelson, M. R. Norman, S. Uchida, and J. Zaanen, From quantum matter to high-temperature superconductivity in copper oxides, Nature **518**, 179 (2015).

[2] D. J. Scalapino, A common thread: The pairing interaction for unconventional superconductors, Rev. Mod. Phys. **84**, 1383 (2012).

[3] Y. Kamihara, T. Watanabe, M. Hirano, and H. Hosono, Iron-Based Layered Superconductor $LaO_{1-x}F_xFeAs$ ($x = 0.05 - 0.12$) with $T_c = 26$ K, Journal of the American Chemical Society **130**, 3296 (2008), **First observation of superconductivity in an iron-arsenide compound.**

[4] I. I. Mazin, D. J. Singh, M. D. Johannes, and M. H. Du, Unconventional Superconductivity with a Sign Reversal in the Order Parameter of $\mathrm{LaFeAsO}_{1-x}\mathrm{F}_x$, Phys. Rev. Lett. **101**, 057003 (2008), **Theoretical proposal of an s^{+-} superconducting state in FeSC mediated by spin fluctuations.**

[5] K. Kuroki, H. Usui, S. Onari, R. Arita, and H. Aoki, Pnictogen height as a possible switch between high-T_c nodeless and low-T_c nodal pairings in the iron-based superconductors, Phys. Rev. B **79**, 224511 (2009), **RPA calculation that shows the impact of the pnictogen height on the superconducting state.**

[6] P. J. Hirschfeld, M. M. Korshunov, and I. I. Mazin, Gap symmetry and structure of Fe-based superconductors, Reports on Progress in Physics **74**, 124508 (2011).

[7] A. V. Chubukov, Pairing Mechanism in Fe-Based Superconductors, Annual Review of Condensed Matter Physics **3**, 57 (2012), **A pedagogical review that compares the RPA and RG approaches to describe superconductivity in FeSC.**

[8] F. Wang and D.-H. Lee, The Electron-Pairing Mechanism of Iron-Based Superconductors, Science **332**, 200 (2011).

[9] K. Haule and G. Kotliar, Coherence–incoherence crossover in the normal state of iron oxypnictides and importance of Hund's rule coupling, New Journal of Physics **11**, 025021 (2009), **Theoretical prediction of a coherence-incoherence crossover caused by the Hund's coupling, which later led to the concept of a Hund metal.**

[10] Z. Yin, K. Haule, and G. Kotliar, Kinetic frustration and the nature of the magnetic and paramagnetic states in iron pnictides and iron chalcogenides, Nature Materials **10**, 932 (2011), **Provides principles for organizing the families of FeSC by their correlation strength and differentiation of the dxy orbitals.**

[11] K. M. Stadler, Z. P. Yin, J. von Delft, G. Kotliar, and A. Weichselbaum, Dynamical mean-field theory plus numerical renormalization-group study of spin-orbital separation in a three-band hund metal, Phys. Rev. Lett. **115**, 136401 (2015).

[12] L. de' Medici, S. R. Hassan, M. Capone, and X. Dai, Orbital-Selective Mott Transition out of Band Degeneracy Lifting, Phys. Rev. Lett. **102**, 126401 (2009).

[13] E. Bascones, B. Valenzuela, and M. J. Calderón, Orbital differentiation and the role of orbital ordering in the magnetic state of Fe superconductors, Phys. Rev. B **86**, 174508 (2012).

[14] R. Yu and Q. Si, Orbital-Selective Mott Phase in Multiorbital Models for Alkaline Iron Selenides $\mathrm{K}_{1-x}\mathrm{Fe}_{2-y}\mathrm{Se}_2$, Phys. Rev. Lett. **110**, 146402 (2013).

[15] L. de' Medici, G. Giovannetti, and M. Capone, Selective Mott Physics as a Key to Iron Superconductors, Phys. Rev. Lett. **112**, 177001 (2014).

[16] A. Georges, L. d. Medici, and J. Mravlje, Strong Correlations from Hund's Coupling, Annual Review of Condensed Matter Physics **4**, 137 (2013).

[17] P. Dai, Antiferromagnetic order and spin dynamics in iron-based superconductors, Rev. Mod. Phys. **87**, 855 (2015).

[18] M. D. Lumsden and A. D. Christianson, Magnetism in Fe-based superconductors, Journal of Physics: Condensed Matter **22**, 203203 (2010), **Topical review that surveys early neutron scattering data on FeSC, including the observation of spin-resonance modes in the superconducting state.**

[19] D. Inosov, J. Park, P. Bourges, D. Sun, Y. Sidis, A. Schneidewind, K. Hradil, D. Haug, C. Lin, B. Keimer, *et al.*, Normal-state spin dynamics and temperature-dependent spin-resonance energy in optimally doped $BaFe_{1.85}Co_{0.15}As_2$, Nature Physics **6**, 178 (2010).

[20] R. M. Fernandes, A. V. Chubukov, and J. Schmalian, What drives nematic order in iron-based superconductors?, Nature Physics **10**, 97 (2014).

[21] E. Fradkin, S. A. Kivelson, M. J. Lawler, J. P. Eisenstein, and A. P. Mackenzie, Nematic Fermi Fluids in Condensed Matter Physics, Annual Review of Condensed Matter Physics **1**, 153 (2010).

[22] J.-H. Chu, H.-H. Kuo, J. G. Analytis, and I. R. Fisher, Divergent nematic susceptibility in an iron arsenide superconductor, Science **337**, 710 (2012), **Elastoresistivity measurements reveal presence of nematic fluctuations across the phase diagram of an FeSC compound.**

[23] A. E. Böhmer, P. Burger, F. Hardy, T. Wolf, P. Schweiss, R. Fromknecht, M. Reinecker, W. Schranz, and C. Meingast, Nematic Susceptibility of Hole-Doped and Electron-Doped $BaFe_2As_2$ Iron-Based Superconductors from Shear Modulus Measurements, Phys. Rev. Lett. **112**, 047001 (2014).

[24] Y. Gallais, R. M. Fernandes, I. Paul, L. Chauvière, Y.-X. Yang, M.-A. Méasson, M. Cazayous, A. Sacuto, D. Colson, and A. Forget, Observation of Incipient Charge Nematicity in $Ba(Fe_{1-X}Co_X)_2As_2$, Phys. Rev. Lett. **111**, 267001 (2013).

[25] P. Zhang, K. Yaji, T. Hashimoto, Y. Ota, T. Kondo, K. Okazaki, Z. Wang, J. Wen, G. D. Gu, H. Ding, and S. Shin, Observation of topological superconductivity on the surface of an iron-based superconductor, Science **360**, 182 (2018), **ARPES measurements reveal surface topological spin-helical states in $FeTe_{1-x}Se_x$.**

[26] D. J. Singh and M.-H. Du, Density Functional Study of $LaFeAsO_{1-x}F_x$: A Low Carrier Density Superconductor Near Itinerant Magnetism, Phys. Rev. Lett. **100**, 237003 (2008).

[27] H. Eschrig and K. Koepernik, Tight-binding models for the iron-based superconductors, Phys. Rev. B **80**, 104503 (2009).

[28] V. Cvetkovic and O. Vafek, Space group symmetry, spin-orbit coupling, and the low-energy effective Hamiltonian for iron-based superconductors, Phys. Rev. B **88**, 134510 (2013).

[29] S. Borisenko, D. Evtushinsky, Z.-H. Liu, I. Morozov, R. Kappenberger, S. Wurmehl, B. Büchner, A. Yaresko, T. Kim, M. Hoesch, *et al.*, Direct observation of spin-orbit coupling in iron-based superconductors, Nature Physics **12**, 311 (2016).

[30] Z. Wang, P. Zhang, G. Xu, L. K. Zeng, H. Miao, X. Xu, T. Qian, H. Weng, P. Richard, A. V. Fedorov, H. Ding, X. Dai, and Z. Fang, Topological nature of the $\mathrm{FeSe_{0.5}Te_{0.5}}$ superconductor, Phys. Rev. B **92**, 115119 (2015).

[31] W. L. Yang, A. P. Sorini, C.-C. Chen, B. Moritz, W.-S. Lee, F. Vernay, P. Olalde-Velasco, J. D. Denlinger, B. Delley, J.-H. Chu, J. G. Analytis, I. R. Fisher, Z. A. Ren, J. Yang, W. Lu, Z. X. Zhao, J. van den Brink, Z. Hussain, Z.-X. Shen, and T. P. Devereaux, Evidence for weak electronic correlations in iron pnictides, Phys. Rev. B **80**, 014508 (2009).

[32] P. Richard, T. Qian, and H. Ding, ARPES measurements of the superconducting gap of Fe-based superconductors and their implications to the pairing mechanism, Journal of Physics: Condensed Matter **27**, 293203 (2015).

[33] A. I. Coldea, Electronic Nematic States Tuned by Isoelectronic Substitution in Bulk $\mathrm{FeSe_{1-x}S_x}$, Frontiers in Physics **8**, 528 (2021).

[34] M. Yi, Y. Zhang, Z.-X. Shen, and D. Lu, Role of the orbital degree of freedom in iron-based superconductors, npj Quantum Materials **2**, 57 (2017).

[35] A. Carrington, Quantum oscillation studies of the Fermi surface of iron-pnictide superconductors, Reports on Progress in Physics **74**, 124507 (2011).

[36] A. I. Coldea, J. D. Fletcher, A. Carrington, J. G. Analytis, A. F. Bangura, J.-H. Chu, A. S. Erickson, I. R. Fisher, N. E. Hussey, and R. D. McDonald, Fermi Surface of Superconducting LaFePO Determined from Quantum Oscillations, Phys. Rev. Lett. **101**, 216402 (2008).

[37] M. Qazilbash, J. Hamlin, R. Baumbach, L. Zhang, D. J. Singh, M. Maple, and D. Basov, Electronic correlations in the iron pnictides, Nature Physics **5**, 647 (2009).

[38] K. Haule, J. H. Shim, and G. Kotliar, Correlated Electronic Structure of $\mathrm{LaO_{1-x}F_xFeAs}$, Phys. Rev. Lett. **100**, 226402 (2008).

[39] S. L. Skornyakov, A. V. Efremov, N. A. Skorikov, M. A. Korotin, Y. A. Izyumov, V. I. Anisimov,

A. V. Kozhevnikov, and D. Vollhardt, Classification of the electronic correlation strength in the iron pnictides: The case of the parent compound $BaFe_2As_2$, Phys. Rev. B **80**, 092501 (2009).

[40] P. Werner, M. Casula, T. Miyake, F. Aryasetiawan, A. J. Millis, and S. Biermann, Satellites and large doping and temperature dependence of electronic properties in hole-doped $BaFe_2As_2$, Nature Physics **8**, 331 (2012).

[41] J. Ferber, K. Foyevtsova, R. Valentí, and H. O. Jeschke, LDA + DMFT study of the effects of correlation in LiFeAs, Phys. Rev. B **85**, 094505 (2012).

[42] G. Lee, H. S. Ji, Y. Kim, C. Kim, K. Haule, G. Kotliar, B. Lee, S. Khim, K. H. Kim, K. S. Kim, K.-S. Kim, and J. H. Shim, Orbital Selective Fermi Surface Shifts and Mechanism of High T_c Superconductivity in Correlated AFeAs (A = Li, Na), Phys. Rev. Lett. **109**, 177001 (2012).

[43] S. V. Borisenko, V. B. Zabolotnyy, D. V. Evtushinsky, T. K. Kim, I. V. Morozov, A. N. Yaresko, A. A. Kordyuk, G. Behr, A. Vasiliev, R. Follath, and B. Büchner, Superconductivity without Nesting in LiFeAs, Phys. Rev. Lett. **105**, 067002 (2010).

[44] L. Fanfarillo, J. Mansart, P. Toulemonde, H. Cercellier, P. Le Fèvre, F. m. c. Bertran, B. Valenzuela, L. Benfatto, and V. Brouet, Orbital-dependent Fermi surface shrinking as a fingerprint of nematicity in FeSe, Phys. Rev. B **94**, 155138 (2016).

[45] L. Ortenzi, E. Cappelluti, L. Benfatto, and L. Pietronero, Fermi-Surface Shrinking and Interband Coupling in Iron-Based Pnictides, Phys. Rev. Lett. **103**, 046404 (2009).

[46] K. Zantout, S. Backes, and R. Valentí, Effect of Nonlocal Correlations on the Electronic Structure of LiFeAs, Phys. Rev. Lett. **123**, 256401 (2019).

[47] J. M. Tomczak, M. van Schilfgaarde, and G. Kotliar, Many-Body Effects in Iron Pnictides and Chalcogenides: Nonlocal Versus Dynamic Origin of Effective Masses, Phys. Rev. Lett. **109**, 237010 (2012).

[48] D. van der Marel and G. A. Sawatzky, Electron-electron interaction and localization in d and f transition metals, Phys. Rev. B **37**, 10674 (1988).

[49] F. Hardy, A. E. Böhmer, D. Aoki, P. Burger, T. Wolf, P. Schweiss, R. Heid, P. Adelmann, Y. X. Yao, G. Kotliar, J. Schmalian, and C. Meingast, Evidence of Strong Correlations and Coherence-Incoherence Crossover in the Iron Pnictide Superconductor KFe_2As_2, Phys. Rev. Lett. **111**, 027002 (2013).

[50] Z. P. Yin, K. Haule, and G. Kotliar, Fractional power-law behavior and its origin in iron-chalcogenide and ruthenate superconductors: Insights from first-principles calculations, Phys. Rev. B **86**, 195141

(2012).

[51] A. Kreisel, P. J. Hirschfeld, and B. M. Andersen, On the Remarkable Superconductivity of FeSe and Its Close Cousins, Symmetry **12**, 1402 (2020).

[52] R. Yu, J.-X. Zhu, and Q. Si, Orbital-selective superconductivity, gap anisotropy, and spin resonance excitations in a multiorbital t-J_1-J_2 model for iron pnictides, Phys. Rev. B **89**, 024509 (2014).

[53] L. Fanfarillo, A. Valli, and M. Capone, Synergy between Hund-Driven Correlations and Boson-Mediated Superconductivity, Phys. Rev. Lett. **125**, 177001 (2020).

[54] P. O. Sprau, A. Kostin, A. Kreisel, A. E. Böhmer, V. Taufour, P. C. Canfield, S. Mukherjee, P. J. Hirschfeld, B. M. Andersen, and J. C. S. Davis, Discovery of orbital-selective Cooper pairing in FeSe, Science **357**, 75 (2017), **STM observation of a strong gap anisotropy in FeSe and proposal of orbital differentiation inside the superconducting state.**

[55] L. C. Rhodes, M. D. Watson, A. A. Haghighirad, D. V. Evtushinsky, M. Eschrig, and T. K. Kim, Scaling of the superconducting gap with orbital character in FeSe, Phys. Rev. B **98**, 180503 (2018).

[56] D. Liu, C. Li, J. Huang, B. Lei, L. Wang, X. Wu, B. Shen, Q. Gao, Y. Zhang, X. Liu, Y. Hu, Y. Xu, A. Liang, J. Liu, P. Ai, L. Zhao, S. He, L. Yu, G. Liu, Y. Mao, X. Dong, X. Jia, F. Zhang, S. Zhang, F. Yang, Z. Wang, Q. Peng, Y. Shi, J. Hu, T. Xiang, X. Chen, Z. Xu, C. Chen, and X. J. Zhou, Orbital Origin of Extremely Anisotropic Superconducting Gap in Nematic Phase of FeSe Superconductor, Phys. Rev. X **8**, 031033 (2018).

[57] Z. Yin, K. Haule, and G. Kotliar, Spin dynamics and orbital-antiphase pairing symmetry in iron-based superconductors, Nature Physics **10**, 845 (2014).

[58] J. Pelliciari, Y. Huang, K. Ishii, C. Zhang, P. Dai, G. F. Chen, L. Xing, X. Wang, C. Jin, H. Ding, *et al.*, Magnetic moment evolution and spin freezing in doped $BaFe_2As_2$, Scientific Reports **7**, 8003 (2017).

[59] M. Wang, C. Zhang, X. Lu, G. Tan, H. Luo, Y. Song, M. Wang, X. Zhang, E. Goremychkin, T. Perring, T. Maier, Z. Yin, K. Haule, G. Kotliar, and P. Dai, Doping dependence of spin excitations and its correlations with high-temperature superconductivity in iron pnictides, Nature Communications **4**, 2874 (2013).

[60] M. H. Christensen, J. Kang, B. M. Andersen, I. Eremin, and R. M. Fernandes, Spin reorientation driven by the interplay between spin-orbit coupling and Hund's rule coupling in iron pnictides, Phys. Rev. B **92**, 214509 (2015).

[61] N. Qureshi, P. Steffens, Y. Drees, A. C. Komarek, D. Lamago, Y. Sidis, L. Harnagea, H.-J. Grafe,

S. Wurmehl, B. Büchner, and M. Braden, Inelastic Neutron-Scattering Measurements of Incommensurate Magnetic Excitations on Superconducting LiFeAs Single Crystals, Phys. Rev. Lett. **108**, 117001 (2012).

[62] Q. Wang, Y. Shen, B. Pan, X. Zhang, K. Ikeuchi, K. Iida, A. Christianson, H. Walker, D. Adroja, M. Abdel-Hafiez, X. Chen, D. Chareev, A. Vasiliev, and J. Zhao, Magnetic ground state of FeSe, Nature Communications **7**, 12182 (2016).

[63] M. D. Lumsden, A. D. Christianson, E. Goremychkin, S. E. Nagler, H. Mook, M. B. Stone, D. L. Abernathy, T. Guidi, G. J. MacDougall, C. de la Cruz, A. Sefat, M. McGuire, B. Sales, and D. Mandrus, Evolution of spin excitations into the superconducting state in $FeTe_{1-x}Se_x$, Nature Physics **6**, 182 (2010).

[64] T. Liu, J. Hu, B. Qian, D. Fobes, Z. Q. Mao, W. Bao, M. Reehuis, S. Kimber, K. Prokeš, S. Matas, D. Argyriou, A. Hiess, A. Rotaru, H. Pham, L. Spinu, Y. Qiu, V. Thampy, A. Savici, J. Rodriguez, and C. Broholm, From (π, 0) magnetic order to superconductivity with (π, π) magnetic resonance in $Fe_{1.02}Te_{1-x}Se_x$, Nature Materials **9**, 718 (2010).

[65] M. N. Gastiasoro and B. M. Andersen, Enhancement of magnetic stripe order in iron-pnictide superconductors from the interaction between conduction electrons and magnetic impurities, Phys. Rev. Lett. **113**, 067002 (2014).

[66] D. K. Pratt, M. G. Kim, A. Kreyssig, Y. B. Lee, G. S. Tucker, A. Thaler, W. Tian, J. L. Zarestky, S. L. Bud'ko, P. C. Canfield, B. N. Harmon, A. I. Goldman, and R. J. McQueeney, Incommensurate Spin-Density Wave Order in Electron-Doped $\mathrm{BaFe_2As_2}$ Superconductors, Phys. Rev. Lett. **106**, 257001 (2011).

[67] J. M. Allred, K. M. Taddei, D. E. Bugaris, M. J. Krogstad, S. H. Lapidus, D. Y. Chung, H. Claus, M. G. Kanatzidis, D. E. Brown, J. Kang, R. M. Fernandes, I. Eremin, S. Rosenkranz, O. Chmaissem, and R. Osborn, Double-Q spin-density wave in iron arsenide superconductors, Nature Physics **12**, 493 (2016).

[68] J. Lorenzana, G. Seibold, C. Ortix, and M. Grilli, Competing Orders in FeAs Layers, Phys. Rev. Lett. **101**, 186402 (2008).

[69] R. M. Fernandes, S. A. Kivelson, and E. Berg, Vestigial chiral and charge orders from bidirectional spin-density waves: Application to the iron-based superconductors, Phys. Rev. B **93**, 014511 (2016).

[70] W. R. Meier, Q.-P. Ding, A. Kreyssig, S. L. Bud'ko, A. Sapkota, K. Kothapalli, V. Borisov, R. Valentí, C. D. Batista, P. P. Orth, R. M. Fernandes, A. I. Goldman, Y. Furukawa, A. E. Böhmer, and P. C.

Canfield, Hedgehog spin-vortex crystal stabilized in a hole-doped iron-based superconductor, npj Quantum Materials **3**, 5 (2018).

[71] Q. Si and E. Abrahams, Strong Correlations and Magnetic Frustration in the High T_c Iron Pnictides, Phys. Rev. Lett. **101**, 076401 (2008).

[72] K. Seo, B. A. Bernevig, and J. Hu, Pairing symmetry in a two-orbital exchange coupling model of oxypnictides, Phys. Rev. Lett. **101**, 206404 (2008).

[73] P. Dai, J. Hu, and E. Dagotto, Magnetism and its microscopic origin in iron-based high-temperature superconductors, Nature Physics **8**, 709 (2012).

[74] I. Eremin and A. V. Chubukov, Magnetic degeneracy and hidden metallicity of the spin-density-wave state in ferropnictides, Phys. Rev. B **81**, 024511 (2010).

[75] R. M. Fernandes and A. V. Chubukov, Low-energy microscopic models for iron-based superconductors: a review, Reports on Progress in Physics **80**, 014503 (2016).

[76] T. Yildirim, Origin of the 150-K Anomaly in LaFeAsO: Competing Antiferromagnetic Interactions, Frustration, and a Structural Phase Transition, Phys. Rev. Lett. **101**, 057010 (2008).

[77] J. Glasbrenner, I. Mazin, H. O. Jeschke, P. Hirschfeld, R. Fernandes, and R. Valentí, Effect of magnetic frustration on nematicity and superconductivity in iron chalcogenides, Nature Physics **11**, 953 (2015).

[78] M. Hirayama, T. Misawa, T. Miyake, and M. Imada, Ab initio Studies of Magnetism in the Iron Chalcogenides FeTe and FeSe, Journal of the Physical Society of Japan **84**, 093703 (2015).

[79] E. Abrahams and Q. Si, Quantum criticality in the iron pnictides and chalcogenides, Journal of Physics: Condensed Matter **23**, 223201 (2011).

[80] T. Shibauchi, A. Carrington, and Y. Matsuda, A quantum critical point lying beneath the superconducting dome in iron pnictides, Annual Review of Condensed Matter Physics **5**, 113 (2014), **Review of the evidence of quantum critical behavior in FeSC, including the observation of a sharp peak in the doping-dependent penetration depth.**

[81] I. M. Hayes, R. D. McDonald, N. P. Breznay, T. Helm, P. J. Moll, M. Wartenbe, A. Shekhter, and J. G. Analytis, Scaling between magnetic field and temperature in the high-temperature superconductor $BaFe_2\,(As_{1-x}P_x)_2$, Nature Physics **12**, 916 (2016).

[82] D. Chowdhury, B. Swingle, E. Berg, and S. Sachdev, Singularity of the London Penetration Depth at Quantum Critical Points in Superconductors, Phys. Rev. Lett. **111**, 157004 (2013).

[83] A. Levchenko, M. G. Vavilov, M. Khodas, and A. V. Chubukov, Enhancement of the London Pene-

tration Depth in Pnictides at the Onset of Spin-Density-Wave Order under Superconducting Dome, Phys. Rev. Lett. **110**, 177003 (2013).

[84] X. Lu, J. Park, R. Zhang, H. Luo, A. H. Nevidomskyy, Q. Si, and P. Dai, Nematic spin correlations in the tetragonal state of uniaxial-strained $BaFe_{2-x}Ni_xAs_2$, Science **345**, 657 (2014), **Inelastic neutron scattering experiments in a detwinned FeSC compound reveal the intertwining between nematic order and spin fluctuations.**

[85] J.-H. Chu, J. G. Analytis, K. De Greve, P. L. McMahon, Z. Islam, Y. Yamamoto, and I. R. Fisher, In-Plane Resistivity Anisotropy in an Underdoped Iron Arsenide Superconductor, Science **329**, 824 (2010).

[86] C. Mirri, A. Dusza, S. Bastelberger, M. Chinotti, L. Degiorgi, J.-H. Chu, H.-H. Kuo, and I. R. Fisher, Origin of the Resistive Anisotropy in the Electronic Nematic Phase of $BaFe_2As_2$ Revealed by Optical Spectroscopy, Phys. Rev. Lett. **115**, 107001 (2015).

[87] T.-M. Chuang, M. P. Allan, J. Lee, Y. Xie, N. Ni, S. L. Bud'ko, G. S. Boebinger, P. C. Canfield, and J. C. Davis, Nematic Electronic Structure in the "Parent" State of the Iron-Based Superconductor $Ca(Fe_{1-x}Co_x)_2As_2$, Science **327**, 181 (2010).

[88] S. Liang, A. Moreo, and E. Dagotto, Nematic State of Pnictides Stabilized by Interplay between Spin, Orbital, and Lattice Degrees of Freedom, Phys. Rev. Lett. **111**, 047004 (2013).

[89] C.-C. Lee, W.-G. Yin, and W. Ku, Ferro-Orbital Order and Strong Magnetic Anisotropy in the Parent Compounds of Iron-Pnictide Superconductors, Phys. Rev. Lett. **103**, 267001 (2009).

[90] W. Lv, F. Krüger, and P. Phillips, Orbital ordering and unfrustrated $(\pi, 0)$ magnetism from degenerate double exchange in the iron pnictides, Phys. Rev. B **82**, 045125 (2010).

[91] C. Fang, H. Yao, W.-F. Tsai, J. Hu, and S. A. Kivelson, Theory of electron nematic order in LaFeAsO, Phys. Rev. B **77**, 224509 (2008).

[92] C. Xu, M. Müller, and S. Sachdev, Ising and spin orders in the iron-based superconductors, Phys. Rev. B **78**, 020501 (2008).

[93] R. M. Fernandes, P. P. Orth, and J. Schmalian, Intertwined Vestigial Order in Quantum Materials: Nematicity and Beyond, Annual Review of Condensed Matter Physics **10**, 133 (2019).

[94] F. Wang, S. A. Kivelson, and D.-H. Lee, Nematicity and quantum paramagnetism in fese, Nature Physics **11**, 959 (2015).

[95] R. M. Fernandes, A. V. Chubukov, J. Knolle, I. Eremin, and J. Schmalian, Preemptive nematic order, pseudogap, and orbital order in the iron pnictides, Phys. Rev. B **85**, 024534 (2012).

[96] E. Gati, L. Xiang, S. L. Bud'ko, and P. C. Canfield, Role of the Fermi surface for the pressure-tuned nematic transition in the $BaFe_2As_2$ family, Phys. Rev. B **100**, 064512 (2019).

[97] R. M. Fernandes, A. E. Böhmer, C. Meingast, and J. Schmalian, Scaling between Magnetic and Lattice Fluctuations in Iron Pnictide Superconductors, Phys. Rev. Lett. **111**, 137001 (2013).

[98] S. Baek, D. Efremov, J. Ok, J. Kim, J. van den Brink, and B. Büchner, Orbital-driven nematicity in FeSe, Nature Materials **14**, 210 (2015).

[99] A. E. Böhmer, K. Kothapalli, W. T. Jayasekara, J. M. Wilde, B. Li, A. Sapkota, B. G. Ueland, P. Das, Y. Xiao, W. Bi, J. Zhao, E. E. Alp, S. L. Bud'ko, P. C. Canfield, A. I. Goldman, and A. Kreyssig, Distinct pressure evolution of coupled nematic and magnetic orders in FeSe, Phys. Rev. B **100**, 064515 (2019).

[100] Y. Suzuki, T. Shimojima, T. Sonobe, A. Nakamura, M. Sakano, H. Tsuji, J. Omachi, K. Yoshioka, M. Kuwata-Gonokami, T. Watashige, R. Kobayashi, S. Kasahara, T. Shibauchi, Y. Matsuda, Y. Yamakawa, H. Kontani, and K. Ishizaka, Momentum-dependent sign inversion of orbital order in superconducting FeSe, Phys. Rev. B **92**, 205117 (2015).

[101] S. Lederer, Y. Schattner, E. Berg, and S. A. Kivelson, Superconductivity and non-Fermi liquid behavior near a nematic quantum critical point, Proceedings of the National Academy of Sciences **114**, 4905 (2017).

[102] A. Klein and A. V. Chubukov, Superconductivity near a nematic quantum critical point: Interplay between hot and lukewarm regions, Phys. Rev. B **98**, 220501 (2018).

[103] T. Worasaran, M. S. Ikeda, J. C. Palmstrom, J. A. W. Straquadine, S. A. Kivelson, and I. R. Fisher, Nematic quantum criticality in an fe-based superconductor revealed by strain-tuning, Science **372**, 973 (2021).

[104] T. Shibauchi, T. Hanaguri, and Y. Matsuda, Exotic Superconducting States in FeSe-based Materials, Journal of the Physical Society of Japan **89**, 102002 (2020).

[105] P. Reiss, D. Graf, A. A. Haghighirad, W. Knafo, L. Drigo, M. Bristow, A. J. Schofield, and A. I. Coldea, Quenched nematic criticality and two superconducting domes in an iron-based superconductor, Nature Physics **16**, 89 (2020).

[106] D. Huang and J. E. Hoffman, Monolayer FeSe on $SrTiO_3$, Annual Review of Condensed Matter Physics **8**, 311 (2017).

[107] H. Hosono, A. Yamamoto, H. Hiramatsu, and Y. Ma, Recent advances in iron-based superconductors toward applications, Materials Today **21**, 278 (2018).

[108] L. Boeri, O. V. Dolgov, and A. A. Golubov, Is $\mathrm{LaFeAsO}_{1-x}\mathrm{F}_x$ an Electron-Phonon Superconductor?, Phys. Rev. Lett. **101**, 026403 (2008).

[109] S. Mandal, R. E. Cohen, and K. Haule, Strong pressure-dependent electron-phonon coupling in FeSe, Phys. Rev. B **89**, 220502 (2014).

[110] J. Lee, F. Schmitt, R. Moore, S. Johnston, Y.-T. Cui, W. Li, M. Yi, Z. Liu, M. Hashimoto, Y. Zhang, *et al.*, Interfacial mode coupling as the origin of the enhancement of T_c in FeSe films on SrTiO_3, Nature **515**, 245 (2014), **Observation of a connection between a substrate phonon mode and the enhancement of superconductivity in monolayer FeSe grown on $\mathbf{SrTiO}_3$.**

[111] R. Thomale, C. Platt, W. Hanke, J. Hu, and B. A. Bernevig, Exotic d-Wave Superconducting State of Strongly Hole-Doped $\mathbf{K}_x\mathrm{Ba}_{1-x}\mathrm{Fe}_2\mathrm{As}_2$, Phys. Rev. Lett. **107**, 117001 (2011).

[112] I. Paul and M. Garst, Lattice Effects on Nematic Quantum Criticality in Metals, Phys. Rev. Lett. **118**, 227601 (2017).

[113] H. Kontani and S. Onari, Orbital-Fluctuation-Mediated Superconductivity in Iron Pnictides: Analysis of the Five-Orbital Hubbard-Holstein Model, Phys. Rev. Lett. **104**, 157001 (2010).

[114] C.-T. Chen, C. Tsuei, M. Ketchen, Z.-A. Ren, and Z. Zhao, Integer and half-integer flux-quantum transitions in a niobium-iron pnictide loop, Nature Physics **6**, 260 (2010).

[115] T. Hanaguri, S. Niitaka, K. Kuroki, and H. Takagi, Unconventional s-wave superconductivity in Fe(Se,Te), Science **328**, 474 (2010).

[116] K. Cho, M. Kończykowski, S. Teknowijoyo, M. A. Tanatar, and R. Prozorov, Using electron irradiation to probe iron-based superconductors, Superconductor Science and Technology **31**, 064002 (2018).

[117] H. Yang, Z. Wang, D. Fang, Q. Deng, Q.-H. Wang, Y.-Y. Xiang, Y. Yang, and H.-H. Wen, In-gap quasiparticle excitations induced by non-magnetic Cu impurities in Na($\mathrm{Fe}_{0.96}\mathrm{Co}_{0.03}\mathrm{Cu}_{0.01}$)As revealed by scanning tunnelling spectroscopy, Nature Communications **4**, 2749 (2013).

[118] K. Okazaki, Y. Ota, Y. Kotani, W. Malaeb, Y. Ishida, T. Shimojima, T. Kiss, S. Watanabe, C.-T. Chen, K. Kihou, C. H. Lee, A. Iyo, H. Eisaki, T. Saito, H. Fukazawa, Y. Kohori, K. Hashimoto, T. Shibauchi, Y. Matsuda, H. Ikeda, H. Miyahara, R. Arita, A. Chainani, and S. Shin, Octet-Line Node Structure of Superconducting Order Parameter in $\mathrm{KFe}_2\mathrm{As}_2$, Science **337**, 1314 (2012), **Direct observation of accidental nodes in a hole-doped FeSC compound via laser ARPES measurements.**

[119] T.-H. Lee, A. V. Chubukov, H. Miao, and G. Kotliar, Pairing Mechanism in Hund's Metal Supercon-

ductors and the Universality of the Superconducting Gap to Critical Temperature Ratio, Phys. Rev. Lett. **121**, 187003 (2018).

[120] W.-C. Lee, S.-C. Zhang, and C. Wu, Pairing State with a Time-Reversal Symmetry Breaking in FeAs-Based Superconductors, Phys. Rev. Lett. **102**, 217002 (2009).

[121] V. Stanev and Z. Tešanović, Three-band superconductivity and the order parameter that breaks time-reversal symmetry, Phys. Rev. B **81**, 134522 (2010).

[122] V. Grinenko, R. Sarkar, K. Kihou, C. Lee, I. Morozov, S. Aswartham, B. Büchner, P. Chekhonin, W. Skrotzki, K. Nenkov, R. Hühne, K. Nielsch, S. L. Drechsler, V. L. Vadimov, M. A. Silaev, P. A. Volkov, I. Eremin, H. Luetkens, and H. H. Klauss, Superconductivity with broken time-reversal symmetry inside a superconducting s-wave state, Nature Physics **16**, 789 (2020).

[123] F. Kretzschmar, B. Muschler, T. Böhm, A. Baum, R. Hackl, H.-H. Wen, V. Tsurkan, J. Deisenhofer, and A. Loidl, Raman-Scattering Detection of Nearly Degenerate s-Wave and d-Wave Pairing Channels in Iron-Based $Ba_{0.6}K_{0.4}Fe_2As_2$ and $Rb_{0.8}Fe_{1.6}Se_2$ Superconductors, Phys. Rev. Lett. **110**, 187002 (2013).

[124] V. K. Thorsmølle, M. Khodas, Z. P. Yin, C. Zhang, S. V. Carr, P. Dai, and G. Blumberg, Critical quadrupole fluctuations and collective modes in iron pnictide superconductors, Phys. Rev. B **93**, 054515 (2016).

[125] Y. Gallais, I. Paul, L. Chauvière, and J. Schmalian, Nematic Resonance in the Raman Response of Iron-Based Superconductors, Phys. Rev. Lett. **116**, 017001 (2016).

[126] F. Tafti, A. Juneau-Fecteau, M.-E. Delage, S. R. De Cotret, J.-P. Reid, A. Wang, X. Luo, X. Chen, N. Doiron-Leyraud, and L. Taillefer, Sudden reversal in the pressure dependence of T_c in the iron-based superconductor KFe_2As_2, Nature Physics **9**, 349 (2013).

[127] S. Rinott, K. B. Chashka, A. Ribak, E. D. L. Rienks, A. Taleb-Ibrahimi, P. Le Fevre, F. Bertran, M. Randeria, and A. Kanigel, Tuning across the BCS-BEC crossover in the multiband superconductor $Fe_{1+y}Se_xTe_{1-x}$: An angle-resolved photoemission study, Science Advances **3**, e1602372 (2017).

[128] H. Lohani, T. Hazra, A. Ribak, Y. Nitzav, H. Fu, B. Yan, M. Randeria, and A. Kanigel, Band inversion and topology of the bulk electronic structure in $FeSe_{0.45}Te_{0.55}$, Phys. Rev. B **101**, 245146 (2020).

[129] P. Zhang, Z. Wang, X. Wu, K. Yaji, Y. Ishida, Y. Kohama, G. Dai, Y. Sun, C. Bareille, K. Kuroda, *et al.*, Multiple topological states in iron-based superconductors, Nature Physics **15**, 41 (2019).

[130] L. Kong, S. Zhu, M. Papaj, H. Chen, L. Cao, H. Isobe, Y. Xing, W. Liu, D. Wang, P. Fan, *et al.*, Half-integer level shift of vortex bound states in an iron-based superconductor, Nature Physics **15**,

1181 (2019).

[131] D. Wang, L. Kong, P. Fan, H. Chen, S. Zhu, W. Liu, L. Cao, Y. Sun, S. Du, J. Schneeloch, R. Zhong, G. Gu, L. Fu, H. Ding, and H.-J. Gao, Evidence for Majorana bound states in an iron-based superconductor, Science **362**, 333 (2018), **STM measurements reveal a zero-bias peak inside vortices of superconducting $FeTe_{1-x}Se_x$ suggestive of Majorana zero modes.**

[132] T. Machida, Y. Sun, S. Pyon, S. Takeda, Y. Kohsaka, T. Hanaguri, T. Sasagawa, and T. Tamegai, Zero-energy vortex bound state in the superconducting topological surface state of Fe(Se,Te), Nature Materials **18**, 811 (2019).

[133] J.-X. Yin, Z. Wu, J. Wang, Z. Ye, J. Gong, X. Hou, L. Shan, A. Li, X. Liang, X. Wu, *et al.*, Observation of a robust zero-energy bound state in iron-based superconductor Fe(Te,Se), Nature Physics **11**, 543 (2015).

[134] C. Chen, K. Jiang, Y. Zhang, C. Liu, Y. Liu, Z. Wang, and J. Wang, Atomic line defects and zero-energy end states in monolayer Fe(Te,Se) high-temperature superconductors, Nature Physics **16**, 536 (2020).

[135] Z. Wang, J. O. Rodriguez, L. Jiao, S. Howard, M. Graham, G. D. Gu, T. L. Hughes, D. K. Morr, and V. Madhavan, Evidence for dispersing 1D Majorana channels in an iron-based superconductor, Science **367**, 104 (2020).

[136] E. J. König and P. Coleman, Crystalline-Symmetry-Protected Helical Majorana Modes in the Iron Pnictides, Phys. Rev. Lett. **122**, 207001 (2019).

[137] R.-X. Zhang, W. S. Cole, and S. Das Sarma, Helical Hinge Majorana Modes in Iron-Based Superconductors, Phys. Rev. Lett. **122**, 187001 (2019).

[138] T. Misawa, K. Nakamura, and M. Imada, Ab Initio Evidence for Strong Correlation Associated with Mott Proximity in Iron-Based Superconductors, Phys. Rev. Lett. **108**, 177007 (2012).

[139] M. Aichhorn, S. Biermann, T. Miyake, A. Georges, and M. Imada, Theoretical evidence for strong correlations and incoherent metallic state in FeSe, Phys. Rev. B **82**, 064504 (2010).

[140] T. Miyake, K. Nakamura, R. Arita, and M. Imada, Comparison of Ab initio Low-Energy Models for LaFePO, LaFeAsO, $BaFe_2As_2$, LiFeAs, FeSe, and FeTe: Electron Correlation and Covalency, Journal of the Physical Society of Japan **79**, 044705 (2010).

[141] N. Zaki, G. Gu, A. Tsvelik, C. Wu, and P. D. Johnson, Time-reversal symmetry breaking in the Fe-chalcogenide superconductors, Proceedings of the National Academy of Sciences **118**, e2007241118 (2021).

[142] L. Kong, L. Cao, S. Zhu, M. Papaj, G. Dai, G. Li, P. Fan, W. Liu, F. Yang, X. Wang, *et al.*, Majorana zero modes in impurity-assisted vortex of LiFeAs superconductor, Nature Communications **12**, 4146 (2021).

[143] U. Karahasanovic and J. Schmalian, Elastic coupling and spin-driven nematicity in iron-based superconductors, Phys. Rev. B **93**, 064520 (2016).

[144] A. P. Dioguardi, M. M. Lawson, B. T. Bush, J. Crocker, K. R. Shirer, D. M. Nisson, T. Kissikov, S. Ran, S. L. Bud'ko, P. C. Canfield, S. Yuan, P. L. Kuhns, A. P. Reyes, H.-J. Grafe, and N. J. Curro, NMR evidence for inhomogeneous glassy behavior driven by nematic fluctuations in iron arsenide superconductors, Phys. Rev. B **92**, 165116 (2015).

[145] B. A. Frandsen, Q. Wang, S. Wu, J. Zhao, and R. J. Birgeneau, Quantitative characterization of short-range orthorhombic fluctuations in FeSe through pair distribution function analysis, Phys. Rev. B **100**, 020504 (2019).

[146] H.-H. Kuo, J.-H. Chu, J. C. Palmstrom, S. A. Kivelson, and I. R. Fisher, Ubiquitous signatures of nematic quantum criticality in optimally doped Fe-based superconductors, Science **352**, 958 (2016).

[147] O. Vafek and A. V. Chubukov, Hund Interaction, Spin-Orbit Coupling, and the Mechanism of Superconductivity in Strongly Hole-Doped Iron Pnictides, Phys. Rev. Lett. **118**, 087003 (2017).

[148] N. Katayama, K. Kudo, S. Onari, T. Mizukami, K. Sugawara, Y. Sugiyama, Y. Kitahama, K. Iba, K. Fujimura, N. Nishimoto, M. Nohara, and H. Sawa, Superconductivity in $Ca_{1-x}La_xFeAs_2$: A Novel 112-Type Iron Pnictide with Arsenic Zigzag Bonds, Journal of the Physical Society of Japan **82**, 123702 (2013).

[149] E. Dagotto, Colloquium: The unexpected properties of alkali metal iron selenide superconductors, Rev. Mod. Phys. **85**, 849 (2013).

[150] S. Wu, B. A. Frandsen, M. Wang, M. Yi, and R. Birgeneau, Iron-Based Chalcogenide Spin Ladder $BaFe_2X_3$ (X = Se, S), Journal of Superconductivity and Novel Magnetism **33**, 143 (2020).

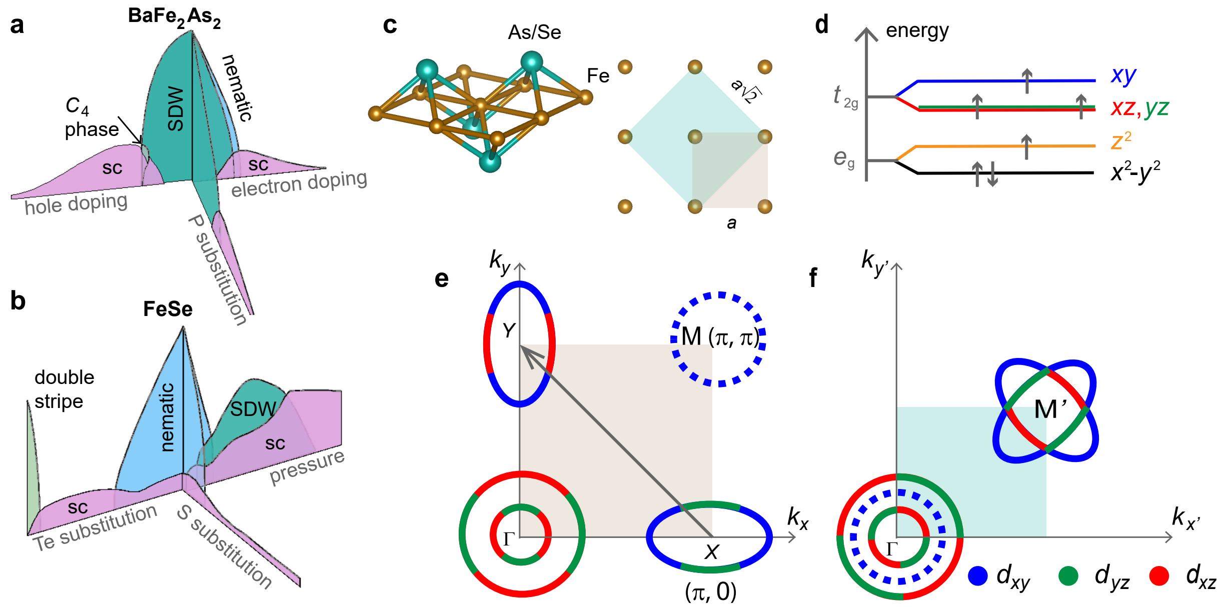

FIG. 1: **General structural and electronic properties**. Phase diagrams of two families of FeSC: (a) $BaFe_2As_2$ [80] and (b) FeSe [33, 51]. Different electronic phases are schematically shown: nematic, spin-density wave (SDW, where nematic order remains present), double-stripe, C_4 magnetic phase, and superconductivity (SC). The tuning parameter can be electron or hole doping, isoelectronic substitution (As/P or Se/S, Se/Te) or applied pressure. (c) The common structure of the FeSC consists of Fe planes and pnictogens (As) or chalcogens (Se) outside the plane. A simplified representation considering a single Fe per unit cell is shown in gray, whereas the crystallographic unit cell containing 2 Fe atoms is shown in green. (d) Schematic representation of the crystal field levels of an isolated Fe^{2+} ion (d^6) inside a distorted $FeAs_4$ tetrahedron [9]. The spins' alignment corresponds to the high spin state, but other configurations are possible. (e) Schematic Fermi surface in the tetragonal phase. It consists of hole pockets at the center and of electron pockets at the corner of the (e) 1-Fe and (f) 2-Fe Brillouin zone. In (f), the two electron pockets fold along the diagonal wave-vector in (e). Colors indicate the dominant orbital character of each band [6]. An additional d_{xy}-dominated hole-pocket (dashed) is shown centered at (π, π) in the 1-Fe zone [$(0, 0)$ in the 2-Fe zone]. The size of this pocket, which is absent in some materials, varies widely across compounds. The momenta in (e) are in units of the inverse lattice constant $1/a$.

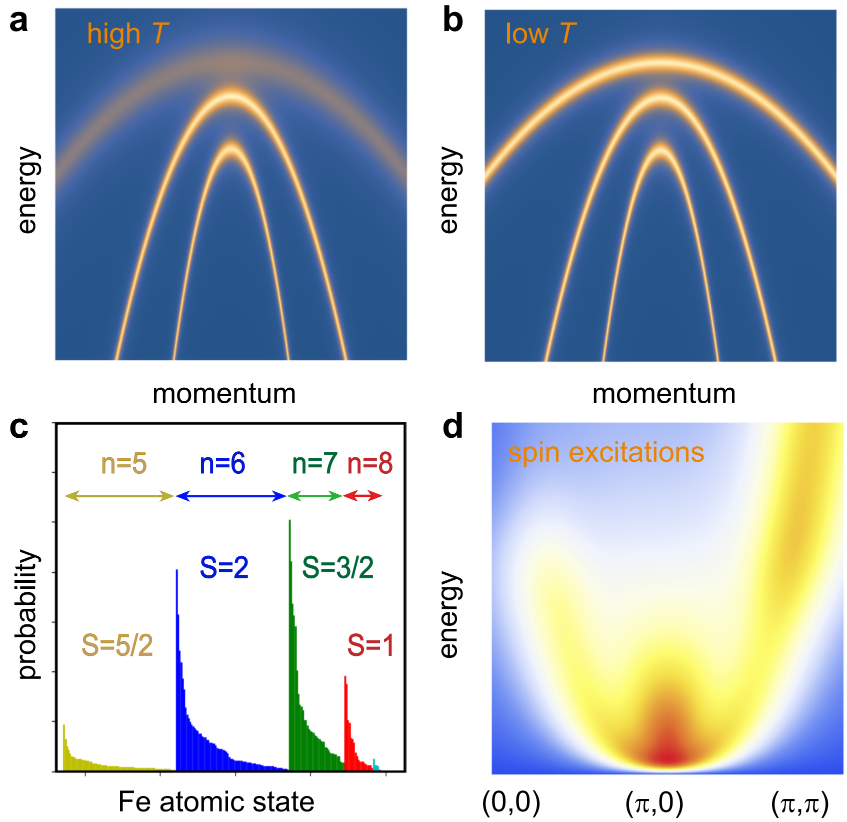

FIG. 2: **Electronic correlations and orbital differentiation**. The energy dispersions of the three hole bands along a high-symmetry direction of the 2-Fe Brillouin zone [Fig. 1(f)] at (a) high temperatures and (b) low temperatures. The topmost hole band, which has d_{xy} character, becomes incoherent at high temperatures, as represented by the faint line. At low temperatures, this band can reestablish its coherence, but its effective mass can remain sizable, as indicated by its flatness. The two other hole bands have d_{xz} and d_{yz} character. Note that the d_{xy} band only crosses the Fermi level in some compounds [Figs. 1(e)-(f)], (c) Histogram of the Fe atomic states in a parent FeSC, as obtained from DMFT calculations [9]. There are 2^{10} possible states involving the $3d$ Fe orbitals. The atomic states are distributed in different colors in the histogram according to their electronic occupation n. Within a given sector n of the histogram, the states are ordered by decreasing probability; in all cases, the higher probability corresponds to the high-spin configuration for that occupation. (d) The typical momentum-resolved spin-excitation spectrum is peaked at different wave-vectors at low energies [in this case, the stripe state $(\pi, 0)$] and high energies [(π, π)].

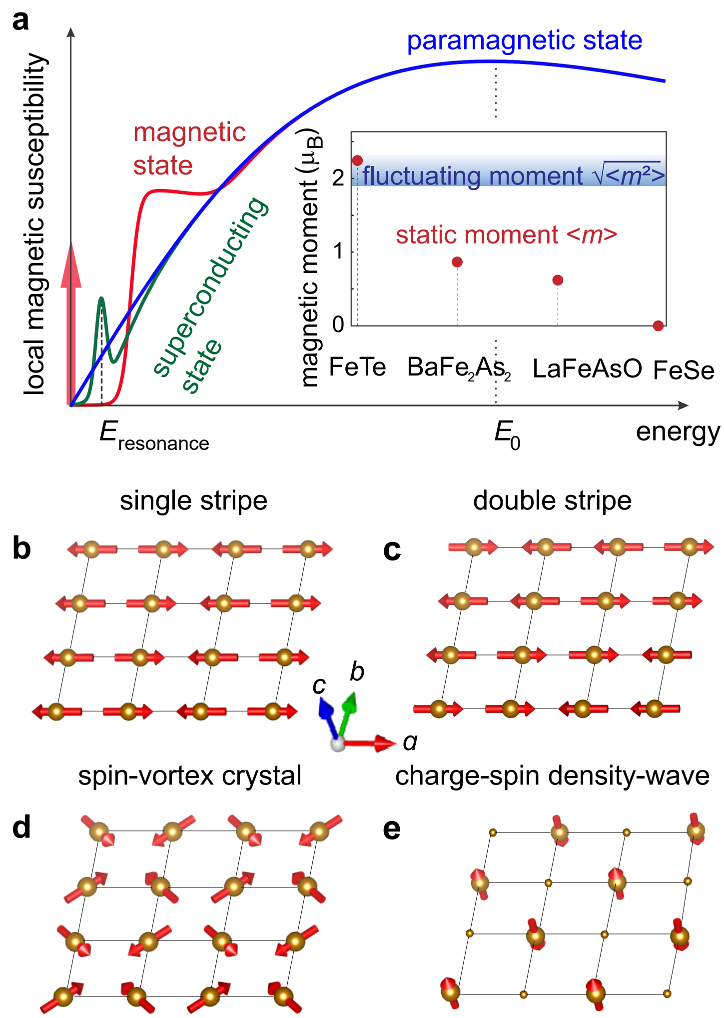

FIG. 3: **Dual local-itinerant nature of magnetism**. (a) Imaginary part of local susceptibility versus energy in a typical FeSC [17]. All FeSC show very similar high energy behavior, but differ at low energies depending on the occurrence of magnetic order (red curve and red arrow, denoting the Bragg peak) or superconductivity (green). The inset shows the variation of the static ordered moment $\langle m \rangle$ across materials, and of the fluctuating local moment, given by the energy-integrated susceptibility $\sqrt{\langle m^2 \rangle}$. (b)-(c) Single-stripe and double-stripe configurations of the Fe spins. The first is realized in most FeSC, whereas the latter, in FeTe. In momentum space, they correspond respectively to Bragg peaks at $(\pi, 0)$ [or $(0, \pi)$] and $(\pi/2, \pi/2)$ in the 1-Fe Brillouin zone. (d)-(e) C_4-symmetric spin configurations observed in electron-doped $CaKFe_4As_4$ [70] and hole-doped $SrFe_2As_2$ [67], respectively. They correspond to a superposition of $(\pi, 0)$ and $(0, \pi)$ wave-vectors resulting in either a non-collinear spin-vortex phase (d), characterized by a staggered spin-vorticity across the Fe square plaquettes, or a charge-spin density-wave phase (e), a non-uniform state with out-of-plane moments in which half of the Fe atoms display vanishing magnetization and a smaller charge density than the average (smaller yellow spheres).

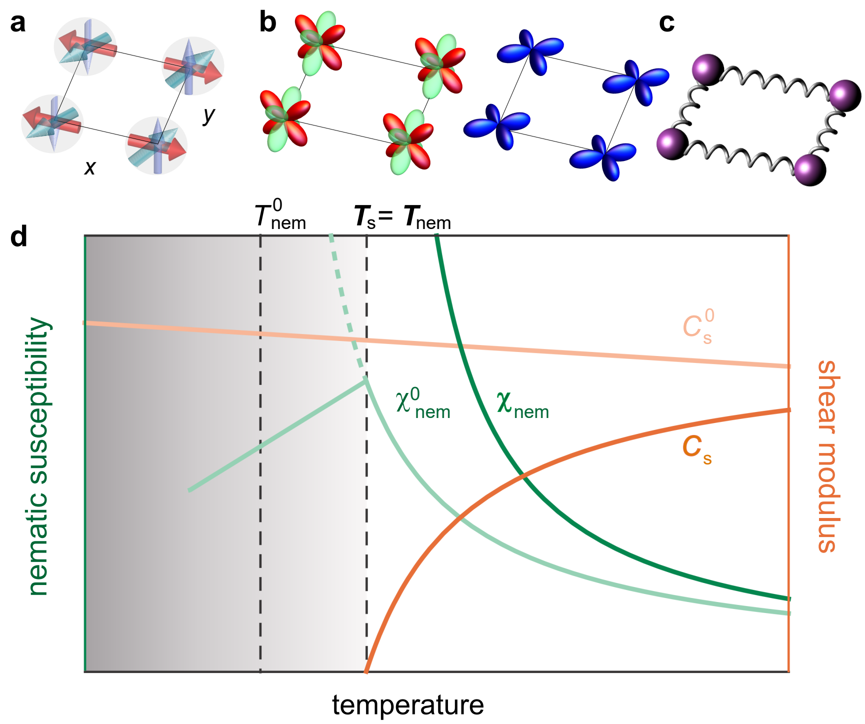

FIG. 4: **Electronic nematic order and its coupling to the lattice**. The nature of the electronic nematic transition remains a matter of investigation, and might involve one or a combination of the following mechanisms [20]. (a) In the case of spin-driven nematic order, partial melting of the stripe magnetic phase results in a state for which $\langle \mathbf{S}_i \rangle = 0$, where $\mathbf{S}_i$ denotes the spin of a specific site i, but for which $\langle \mathbf{S}_i \cdot \mathbf{S}_{i+x} \rangle = - \langle \mathbf{S}_i \cdot \mathbf{S}_{i+y} \rangle$. (b) In the case of orbitally-driven nematic order, interactions lead to a finite difference in the on-site occupancy of orbitals d_{xz} and d_{yz} (denoted by red and green on the left panel) and/or in the d_{xy} orbital hopping (blue, right panel). Symmetry ensures that all these order parameters take on a finite value in the nematic state. In all cases, an associated bare (unrenormalized) nematic susceptibility $\chi^0_{\rm nem}$ can be measured via a number of experimental techniques [22–24]. Coupling to the lattice results in a spontaneous strain with the same symmetry (i.e. a concomitant ferroelastic structural phase transition) at $T_{\rm s} = T_{\rm nem}$ [panel (c)], occurring at a slightly higher temperature than the bare nematic transition temperature $T^0_{\rm nem}$. It also leads to a renormalization of the nematic susceptibility $\chi_{\rm nem}$ for temperatures above $T_{\rm s}$, and a softening of the elastic modulus $C_{\rm s}$ in the same symmetry channel from its bare value $C^0_{\rm s}$ [panel (d)]. Grey shading indicates the magnitude of the nematic order parameter.

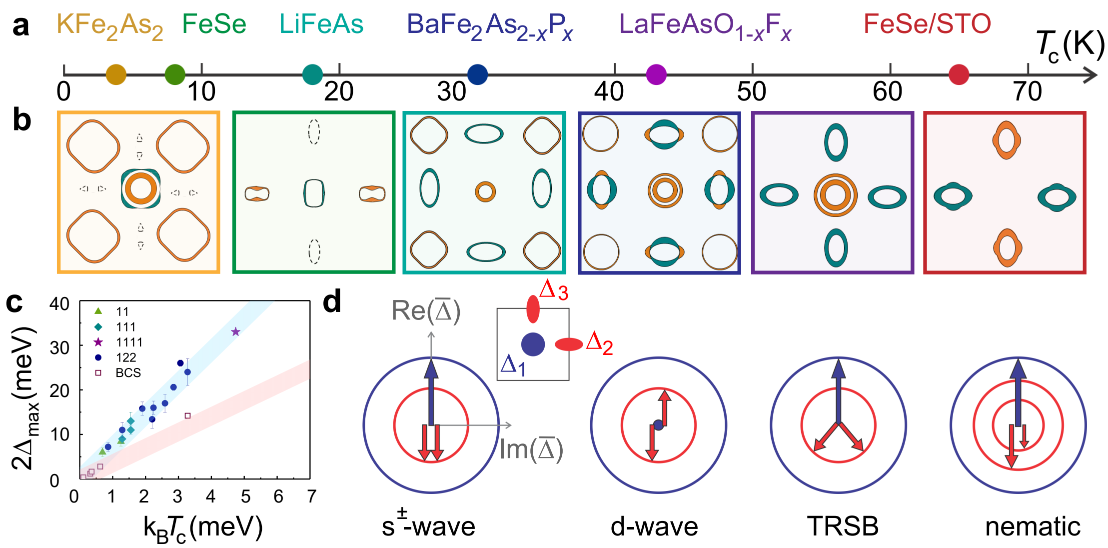

FIG. 5: **Superconducting gap structures and gap symmetries**. (a) Superconducting critical temperatures, T_{c}, of six canonical Fe-based superconductors. (b) Schematic gap structures for these materials in the 1-Fe Brillouin zone (borders colored according to (a)) based on weak-coupling calculations, ARPES, and STM experiments (see [6, 7, 118] and references therein). The line thickness represents the magnitude of the gap, whereas the green and orange colors denote different signs. (c) Ratio between twice the maximum gap ($2\Delta_{\mathrm{max}}$, based on ARPES data) and $k_B T_{\mathrm{c}}$ of FeSC, compared to that of conventional superconductors [119]. Here, k_B is the Boltzmann constant. Colored symbols correspond to some of the materials labeled in (a). The open square symbols correspond to conventional BCS superconductors. (d) Possible superconducting ground states realized in a three-band toy model with repulsive inter-band interactions [75, 121, 122]. The red (blue) arrows are associated with the complex value of the gap averaged around the electron (hole) pockets, $\bar{\Delta}$ (see inset). TRSB denotes time-reversal symmetry breaking. The electron-pockets gaps have distinct averaged values in the nematic case.

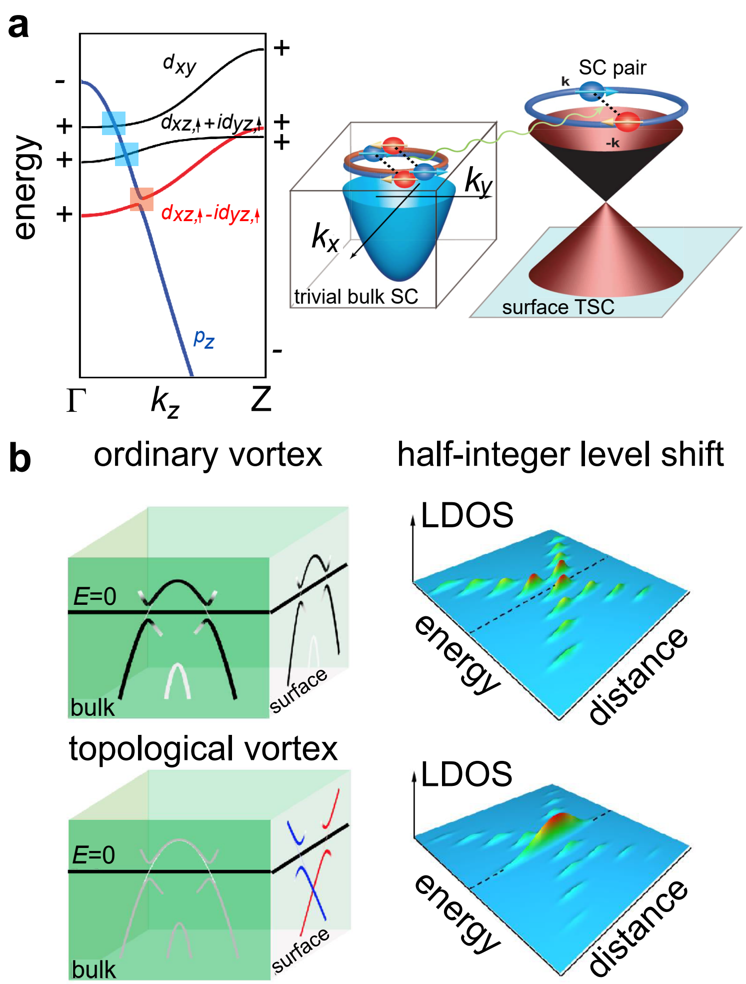

FIG. 6: **Band inversion and topological phenomena.** (a) The topological p-d band inversion in the FeSC is illustrated in the left panel. The downward shift of the p_z-orbital band along the Γ-Z direction causes different topological phenomena such as bulk Dirac semimetal states (blue region) and helical Dirac surface states (orange region), depending on whether it crosses the d_{xy} and $(d_{xz,\uparrow} + id_{yz,\uparrow})$ bands or the $(d_{xz,\uparrow} - id_{yz,\uparrow})$ band, respectively. The bands $(d_{xz,\uparrow} \pm id_{yz,\uparrow})$ arise from the spin-orbit coupling between the degenerate d_{xz} and d_{yz} Fe orbitals in Fig. 1(d), and have total angular momentum $3/2$ (plus sign) and $1/2$ (minus sign) [136]; thus, only the former can hybridize with the p_z band, since the latter has angular momentum $1/2$. The right panel illustrates the topological superconductivity induced on the surface Dirac states by the bulk superconducting state. Figure reproduced from [25]. (b) In the quantum limit, which is achievable in some FeSC, discrete levels can be observed inside a vortex by probing the local density of states (LDOS) via STM. In an ordinary vortex (upper panels), these bound states are all at finite energies, whereas in a topological vortex (lower panels), a sharp zero-energy mode, called a Majorana zero mode, appears well separated from the other bound states. Figure reproduced from [130].